Atmos. Meas. Tech., 8, 579–592, 2015
www.atmos-meas-tech.net/8/579/2015/
doi:10.5194/amt-8-579-2015

Atmospheric Measurement Techniques
Open Access

First continuous measurements of δ^{18}O-CO_2 in air with a Fourier transform infrared spectrometer

S. N. Vardag[1], S. Hammer[1], M. Sabasch[1], D. W. T. Griffith[2], and I. Levin[1]

[1]Institut für Umweltphysik, Heidelberg University, Heidelberg, Germany
[2]Department of Chemistry, University of Wollongong, Wollongong, Australia

Correspondence to: S. N. Vardag (svardag@iup.uni-heidelberg.de)

Received: 15 May 2014 – Published in Atmos. Meas. Tech. Discuss.: 3 July 2014
Revised: 27 October 2014 – Accepted: 7 January 2015 – Published: 4 February 2015

Abstract. The continuous in situ measurement of δ^{18}O in atmospheric CO_2 opens a new door to differentiating between CO_2 source and sink components with high temporal resolution. Continuous ^{13}C–CO_2 measurement systems have already been commercially available for some time, but until now, only few instruments have been able to provide a continuous measurement of the oxygen isotope ratio in CO_2. Besides precise $^{13}C/^{12}C$ observations, the Fourier transform infrared (FTIR) spectrometer is also able to measure the $^{18}O/^{16}O$ ratio in CO_2, but the precision and accuracy of the measurements have not yet been evaluated. Here we present a first analysis of δ^{18}O-CO_2 (and δ^{13}C-CO_2) measurements with the FTIR analyser in Heidelberg. We used Allan deviation to determine the repeatability of δ^{18}O-CO_2 measurements and found that it decreases from 0.25 ‰ for 10 min averages to about 0.1 ‰ after 2 h and remains at that value up to 24 h. We evaluated the measurement precision over a 10-month period (intermediate measurement precision) using daily working gas measurements and found that our spectrometer measured δ^{18}O-CO_2 to better than 0.3 ‰ at a temporal resolution of less than 10 min. The compatibility of our FTIR-spectrometric measurements to isotope-ratio mass-spectrometric (IRMS) measurements was determined by comparing FTIR measurements of cylinder gases and ambient air with IRMS measurements of flask samples, filled with gases of the same cylinders or collected from the same ambient air intake. Two-sample t tests revealed that, at the 0.01 significance level, the FTIR and the IRMS measurements do not differ significantly from each other and are thus compatible. We describe two weekly episodes of ambient air measurements, one in winter and one in summer, and discuss what potential insights and new challenges combined highly resolved CO_2, δ^{13}C-CO_2 and δ^{18}O-CO_2 records may provide in terms of better understanding regional scale continental carbon exchange processes.

1 Introduction

Quantitative understanding of the processes governing the carbon cycle is vital in order to assess the impact and fate of increasing anthropogenic CO_2 emissions to the atmosphere. The stable isotopes in CO_2 can provide information about the fluxes between the different carbon reservoirs, such as the atmosphere, the biosphere and the oceans. $^{13}CO_2$ measurements can be used to distinguish between terrestrial biosphere and marine fluxes (Keeling et al., 1989; Ciais et al., 1995), and are also used as a tracer for anthropogenic emissions, as most fossil fuel CO_2 emissions are depleted in ^{13}C relative to those of the biosphere (Tans, 1981). The interpretation of atmospheric δ^{18}O-CO_2 is more complex, since ^{18}O in CO_2 is strongly coupled to the water cycle (e.g. Francey and Tans, 1987; Farquhar et al., 1993; Cuntz et al., 2003a; 2003b, Buenning et al., 2014). During CO_2 exchange with soil and leaves, the ^{18}O isotopes of CO_2 are exchanged with those of H_2O (Hesterberg and Siegenthaler, 1991). Carbonic anhydrase facilitates the equilibration with leaf water (Gillon and Yakir, 2001; Farquhar et al., 1993). The isotopic composition of soil water is determined by the isotopic composition of precipitation, which itself has strong spatial variations (IAEA/WMO GNIP database available at http://isohis.iaea.org). Since precipitation at higher latitudes is depleted in ^{18}O (Dansgaard, 1964), the soil water and consequently

the CO_2 from root respiration and heterotrophic respiration is also depleted in ^{18}O at higher latitudes (Farquhar et al., 1993). The soil invasion flux will further influence the apparent soil respiration signature as the CO_2 diffuses into the soil, partially equilibrates with soil water and retro-diffuses out of the soil with a new isotopic composition (Tans, 1998; Miller et al., 1999). Isotopic exchange during soil invasion might even be enhanced due to carbonic anhydrase in soils (Wingate et al., 2009). Miller et al. (1999) reported that in most settings and especially in dry ground and for short residence times of air close to the soil surface (corresponding to high boundary layer mixing heights), the effect will be smaller than 5 ‰. Due to ^{18}O enrichment during evapotranspiration, the plant leaf water is enriched in ^{18}O relative to the soil water (Farquhar et al., 1993). During photosynthesis, CO_2 equilibrates with leaf water and about two-thirds of the CO_2 retro-diffuses into the atmosphere without being assimilated (Tans, 1998). The retro-diffused CO_2 changes the atmospheric δ^{18}O-CO_2 value, depending on the isotopic signature of the leaf water. In central Europe, we expect the discrimination against ^{18}O during net CO_2 assimilation to be positive (Farquhar et al., 1993; Cuntz et al. 2003b; Wingate et al., 2009). Still et al. (2009), Welp et al. (2011) and Buenning et al. (2014) have studied the susceptibility of atmospheric δ^{18}O-CO_2 to environmental parameters, such as precipitation, relative humidity, temperature, solar radiation and cloud cover, and estimated the influences of these parameters on the atmospheric δ^{18}O-CO_2 using regional and global scale models. They also assessed the effect of the isotopic composition of precipitation and water vapour. They found that many of these parameters should not be neglected when quantifying biospheric gross ^{18}O-CO_2 fluxes. They also highlight the complexity and the large uncertainties of the processes and sensitivities influencing atmospheric δ^{18}O-CO_2. Thus, in order to understand atmospheric δ^{18}O-CO_2 measurements in all their complexity, information about the regional isotopic composition of precipitation, environmental parameters such as temperature and water vapour deficit and a comprehensive land-surface model are necessary (Yakir and Wang, 1996; Ciais et al., 1997; Langendörfer et al., 2002; Cuntz et al., 2003a; Buenning et al., 2014).

The first step to understanding the ^{18}O-CO_2 fluxes to and from the terrestrial biosphere is to make reliable and comparable measurements at high temporal resolution. However, measurements via isotope-ratio mass-spectrometry (IRMS) are elaborate and time-consuming, limiting the number of continuous records of ^{18}O in CO_2 that exist to date (Flanagan et al., 1997; Langendörfer et al., 2002; Bowling et al., 2003; Pataki et al., 2003). A quantum cascade laser-based absorption spectrometer measuring $^{12}C^{16}O^{16}O$,$^{13}C^{16}O^{16}O$ and $^{12}C^{16}O^{18}O$ with a high temporal resolution provided first continuous records (Tuzson et al., 2011; Sturm et al., 2013). $^{12}C^{16}O^{16}O$ and $^{13}C^{16}O^{16}O$ have also been determined by Fourier transform infrared (FTIR) spectroscopy in several previous studies (e.g. Esler et al., 2000; Mohn et al., 2008; Cambaliza, 2010; Griffith et al., 2012). In principle, FTIR spectroscopy can also provide continuous measurements of $^{12}C^{16}O^{18}O$. However, in their original study, Esler et al. (2000) remarked that the degree of precision is too poor for a useful determination in natural abundances using a 1 cm^{-1} resolution spectrometer. Given improvements in the instrumentation and spectral analysis methods since that time, we have revisited the practicality of continuous measurements of $\delta^{18}O$ in CO_2 using FTIR spectroscopy.

The scope of this manuscript is to answer two important questions: first, is it possible to measure δ^{18}O-CO_2 using FTIR spectroscopy, and if yes, how well can we measure it in terms of precision, accuracy and compatibility to conventional IRMS observations? Second, what insight into regional scale carbon exchange processes can one gain from a highly resolved δ^{18}O-CO_2 record (along with the continuous CO_2, CO and δ^{13}C-CO_2 records) in the catchment area of our measurement site?

2 FTIR measurement principle and calibration procedure

The in situ FTIR analyser used in Heidelberg was developed and built at the University in Wollongong, Australia and is described in detail by Griffith et al. (2012) and Hammer et al. (2013a). It was used during two travelling instrument campaigns by Hammer et al. (2013b) and Vardag et al. (2014) for CO_2, CH_4 and N_2O measurements. Briefly, the FTIR spectrometer obtains a broadband transmittance spectrum of the sample air as the ratio of the infrared spectra measured with and without a sample in the optical cell. The measured transmittance spectrum is fitted by non-linear least squares using the program MALT (Multi-Layer Absorption Transmittance) to model the spectrum (Griffith, 1996; Griffith et al., 2012). The model adjusts sample composition and instrument parameters to obtain the best fit to the measured spectrum, and the best-fit sample concentrations are taken as the retrieved values.

The analyser is a prototype of the now commercially available Spectronus FTIR trace gas analyser (Ecotech, Knoxfield, Australia). While functionally equivalent, there are some component differences. The FTIR spectrometer is an IRcube (Bruker Optics, Ettlingen, Germany) coupled to a glass multipass White cell (model 24 PA, IRanalysis Inc., Anaheim, CA) with 3.5 L volume and 24 m optical path. Spectra were recorded at 1 cm^{-1} resolution and typically coadded to 3 min averages (approximately one cell exchange time at the typical flow rate). The sample handling system comprises four selectable inlets, an optional dryer (Nafion, Permapure PD-100T-24SS), followed by a granulated magnesium perchlorate trap), two mass flow controllers (model D-5111, Bronkhorst, Germany) and a four-head diaphragm vacuum pump (model MV2, Vacuubrand, Germany). One mass flow controller upstream of the cell controls sample air-

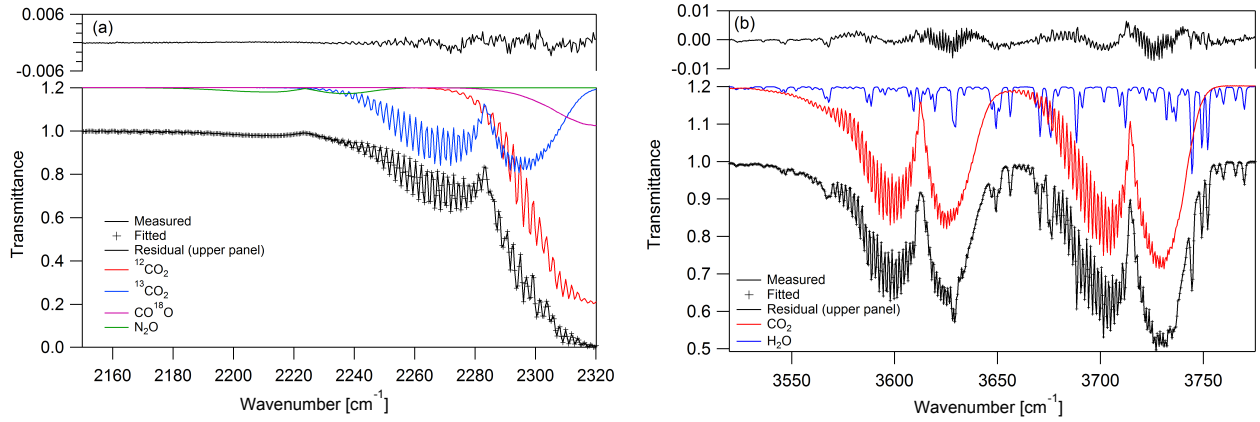

Figure 1. (a) Spectra of CO_2 isotopologues and N_2O in the 2150–2320 cm^{-1} region. The coloured traces show the individual isotopologues, the black spectra are a measured air spectrum (black line), calculated best-fit spectrum (+ symbols) and the fitting residual (black, upper panel). **(b)** Spectrum including CO_2 and H_2O near 3600 cm^{-1}. The individual trace gas and isotopologue spectra are shifted by 0.2 upwards for clarity.

flow, while the other downstream of the cell actively controls pressure via a proportional–integral software control loop to better than ±0.1 hPa. The FTIR housing and the cell are both thermostated and stable within 0.01 °C (1σ). A Windows PC controls sample flow, spectrum collection and online analysis. Sample air is delivered to the analyser at 1500–1800 hPa pressure through a clean diaphragm pump (model N86K.18, KNF Neuberger, Freiburg, Germany). In this work all measurements of both air samples and tank gases were dried (< 10 µmol mol^{-1} water vapour) and made at 1100 hPa pressure, 30 °C and a flow of 1 SLPM (standard litre per minute). The measurements were performed in the laboratory under stable temperature conditions (±1 °C).

Figure 1a shows the CO_2 isotopologue components (coloured traces) of the infrared absorption spectrum of air in the 2150–2320 cm^{-1} spectral region routinely used for CO_2 FTIR analysis by the analyser (Griffith et al., 2012). The black traces show a measured spectrum and typical fit to the composite air spectrum including $^{12}C^{16}O_2$, $^{13}C^{16}O_2$ and $^{12}C^{18}O^{16}O$. Although the $^{12}C^{18}O^{16}O$ isotopologue is heavily overlapped by the parent and $^{13}C^{16}O_2$ isotopologues, its contribution to the total absorption is significant and repeatable and provides the basis for quantification of this isotopologue. The upper panel of Fig. 1a shows a typical spectral residual which is well above the detector noise level above 2240 cm^{-1}. This residual is systematic and constant in shape from spectral fit to fit. The MALT spectrum calculation model is not able to improve this fit, which may be due to either (or both) an imperfect instrument line shape (ILS) or actual line shapes, which are not Voigt shaped as assumed in the model. To investigate the ILS contribution further, we have recorded spectra of air under the same conditions (temperature, pressure, resolution, cell path length) in a Bruker IFS 125/HR spectrometer at the University of Wollongong. This high resolution spectrometer is maintained in a well-aligned condition as part of the Total Carbon Column Observing Network (TCCON, Wunch et al., 2011) and its ILS is well characterised through high resolution test cell measurements (Hase et al., 2013) to be very close to the theoretically ideal shape calculated in the MALT model (modulation efficiency > 0.99, phase error < 0.5°). Fitting these IFS 125/HR spectra resulted in residuals very similar in shape and magnitude to that in Fig. 1a (upper panel), which indicates that imperfect ILS is not the primary cause of the lack of fit. To investigate the possible effects of non-Voigt molecular line shapes, typical FTIR analyser spectra were fitted with two independent spectrum fitting models, GFIT (Geoff Toon, Jet Propulsion Laboratory) and PROFITT (Frank Hase, Karlsruhe Institute of Technology). These spectrum models optionally extend to non-Voigt line shapes including effects of speed dependent cross sections, line narrowing and line mixing (e.g. Ngo et al., 2013). Using several different line shape models did not remove the spectral residuals – in some cases they were slightly reduced or of different shape, but total residuals were reduced by at most 25 %.

Thus, from these two tests we conclude that the residuals are not primarily due to an imperfect instrument line shape, but rather due to the inadequacy of currently available line shape models for the calculation. The imperfect fit is exacerbated by the fact that the residuals are dominated by absorption in the line wings of strongly absorbed lines, which are the least accurately modelled. We must therefore accept the imperfect fits as unavoidable until further advances in line shape models become available. If $^{12}C^{18}O^{16}O$ is removed from the fit, the residuals are two to three times larger; in this case, the least squares fit routine adjusts the amounts of $^{12}C^{16}O_2$ and $^{13}C^{16}O_2$ in the fit by unrealistic amounts to attempt to minimise the residual. The results in this paper show that the $^{12}C^{18}O^{16}O$ amount retrieved from fitting these

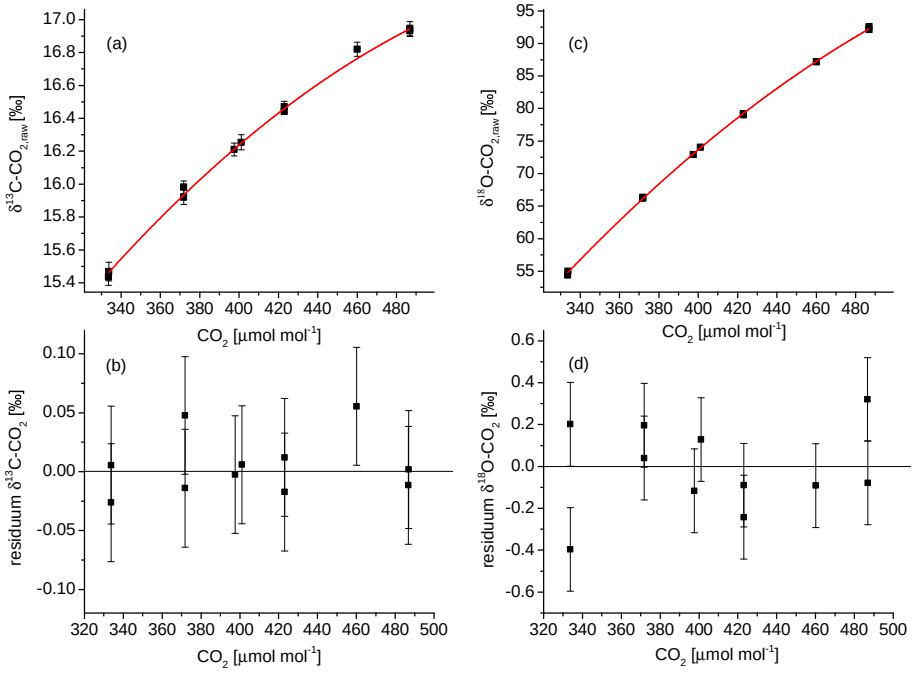

Figure 2. CO_2 dependence of raw δ^{13}C-CO_2 and δ^{18}O-CO_2 (**a** and **b**) and their residuals from the cubic fit (**b** and **d**). The experimental results shown here were obtained in August 2012; the same experiment was repeated in March 2014 and showed no significant difference to the earlier measurements.

spectra, despite the residuals, provides a consistent basis for quantification of this isotopologue.

Total CO_2 can also be retrieved from the region around 3600 cm^{-1} without isotopic discrimination. The fit to this region is shown in Fig. 1b, from Griffith et al. (2012). Retrieval of CO_2 from this region is more precise (i.e. lower noise, better repeatability) than that of $^{12}C^{16}O_2$ near 2300 cm^{-1}, firstly because the bands are not saturated and are of near optimum absorption (50 %), and secondly, because the whole bands have lower temperature sensitivity due to the inclusion of both high and low-J lines with both positive and negative temperature sensitivity. As detailed below, the total CO_2 retrieval, scaled if required, can be used as a proxy for $^{12}C^{16}O_2$ in isotopic calculations with acceptable accuracy.

2.1 Data evaluation and calibration

In the following, we describe the data evaluation and calibration procedure for the isotopologue ratio δ^{18}O-CO_2, but the procedure is analogous for δ^{13}C-CO_2.

Step 1: Calculate the raw δ^{18}O-CO_2 value from FTIR measurements

The FTIR computes the raw δ^{18}O-CO_2 value using the ratio of the raw value of the rare isotopologue and the raw value of the common isotopologue:

$$\delta^{18}\text{O-CO}_{2\text{HITRAN}} = \left[\frac{\left(\frac{^{12}C^{18}O^{16}O_{raw}}{^{12}C^{16}O^{16}O_{raw}}\right)_{sample}}{R_{HITRAN}} - 1 \right] \cdot 1000\ ‰ \qquad (1)$$

with $R_{HITRAN} = 0.0040104$ (Rothman et al., 2005). For ^{13}C, the equivalent value of R_{HITRAN} is 0.0112372.

Following Coplen (2011) and common usage, we use the terminology δ^{18}O-CO_2, even though the δ-notation is originally defined with the isotope ratio (in contrast to isotopologue ratio). The FTIR analysis implicitly uses the HITRAN scale (Rothman et al., 2005), which is referred to Vienna Pee Dee Belemnite (VPDB) for δ^{13}C and to Vienna Standard Mean Ocean Water (VSMOW) for δ^{18}O; during the calibration (step 3) the final reference scale of the calibrated data can be changed to any other scale. We chose the VPDB scale for δ^{13}C-CO_2 ($(^{13}C^{16}O_2/^{12}C^{16}O_2)_{VPDB} = 0.0112372$) and VPDB-$CO_2$ scale for δ^{18}O-CO_2 ($(^{12}C^{18}O^{16}O/^{12}C^{16}O_2)_{VPDB-CO_2} = 0.0041767$) following Allison et al. (1995). We abbreviate δ^{13}C-CO_2 and δ^{18}O-CO_2 on the VPDB-CO_2 scale with δ^{13}C-$CO_{2,VPDB}$ and δ^{18}O-$CO_{2,VPDB}$ respectively.

Step 2: Cross-sensitivity and interspecies interference corrections

To first order, the fitting software MALT takes into account pressure, temperature and interspecies overlapping absorp-

Table 1. Interspecies interference and cross-sensitivity correction factors for δ^{13}C-CO_2 and δ^{18}O-CO_2 used in Eqs. (2) and (3). Reference values were $T_{ref} = 31.8\,°C$, $F_{ref} = 1.0$ SLPM, $P_{ref} = 1100$ hPa and $H_2O_{ref} = 0$ µmole mole^{-1}, for temperature, flow, pressure and water vapour content, respectively.

	δ^{13}C-CO_2	δ^{18}O-CO_2
dC_{raw}/dT [‰ °C^{-1}]	0.127	4.256
dC_{raw}/dF [‰ SLPM^{-1}]	−0.91424	−2.92166
dC_{raw}/dP [‰ hPa^{-1}]	0.00249	−0.18694
dC_{raw}/dH_2O [‰ (µmole mole^{-1})$^{-1}$]		
	0	0
a [‰]	−10.344	−252.786
b [‰ (µmole mole^{-1})$^{-1}$]	0.0461902	1.162269
c [‰ (µmole mole^{-1})$^{-2}$]	−0.0000658108	−0.00179787
d [‰ (µmole mole^{-1})$^{-3}$]	0.000000034299	0.000001093919

tion bands in the fit. However, small second order effects remain due to real imperfections in temperature and pressure measurements, spectrometer instrumental line shape and the assumption of the MALT models (such as Voigt line shapes, see above), necessitating small empirical corrections to the raw measured mole fraction (C_{raw}) (Griffith et al., 2012; Hammer et al., 2013a). A cross-sensitivity correction for sample temperature (T) and pressure (P), H_2O amount and flow rate (F), as well as an interspecies-sensitivity correction for CO_2 mole fraction (corr(CO_2)) is applied for every measurement following Eq. (2):

$$C_{corr} = \frac{dC_{raw}}{dT} \cdot (T - T_{ref}) - \frac{dC_{raw}}{dF} \cdot (F - F_{ref}) - \frac{dC_{raw}}{dP} \cdot (P - P_{ref}) - \frac{dC_{raw}}{dH_2O} \cdot (H_2O - H_2O_{ref}) - \mathrm{corr}(CO_2) \quad (2)$$

Where P_{ref}, T_{ref}, etc. are the reference values to which pressure, temperature etc. are corrected, and the CO_2 correction follows:

$$\mathrm{corr}(CO_2) = a + b \cdot C_{raw} + c \cdot {C_{raw}}^2 + d \cdot {C_{raw}}^3 \quad (3)$$

Table 1 lists all cross-sensitivity parameters and CO_2-interspecies interference corrections.

Hammer et al. (2013a) describe in detail the set-up of the experiment to determine the CO_2 sensitivity. We use a cubic fit to describe the CO_2 interspecies correction (Fig. 2a and b; coefficient of determination $R^2 = 0.99$ for δ^{13}C-CO_2 and for δ^{18}O-CO_2), with residuals showing no further concentration dependence (Fig. 2b and d).

Step 3: Calibration

The cross-sensitivity corrected data are calibrated on the VPDB gas scale using a linear instrument response function (typically linear to the degree of $R^2 = 0.9998$). We derive the calibration response function weekly from three reference tanks with known values for CO_2, δ^{13}C-CO_2 and δ^{18}O-CO_2. Our reference standards span ranges from about 370 to 470 µmol mol^{-1} for CO_2 mole fraction, a $\delta^{13}C\text{-}CO_{2,VPDB}$ range from −8.7 to −12.8 ‰ and a $\delta^{18}O\text{-}CO_{2,VPDB}$ range from −1.9 to −5.0 ‰ as determined by the Heidelberg IRMS (Neubert, 1998).

Step 4: Smoothed working standard correction

We have found that regular measurements of different cylinder gases on the FTIR analyser show small but correlated sub-weekly variations of δ^{18}O-CO_2. One can thus use a smoothed working standard correction in order to account for these small instrumental variations on a sub-weekly time scale. For this purpose, we smooth daily working gas measurements using a 10-point moving average and interpolate the residual variation to the date of sample measurement using a cubic spline interpolation. We then subtract the smoothed residual variations from the long-term mean value of this gas vs. the reference standards from all sample measurements. By performing this correction, typically less than 0.2 ‰, the standard deviation of a weekly measured target or surveillance gas reaches about 0.2 ‰ for δ^{18}O-CO_2. Step 4 is not obligatory, but further increases the precision of the measurement. In the data presented in Sect. 4, we have applied this smoothed working standard correction.

Figure 3 illustrates the application for the entire calibration procedure. For δ^{13}C-CO_2, Fig. 3 shows raw (a), corrected (b) and calibrated (c) FTIR measurements against IRMS reference values of δ^{13}C-CO_2, and Fig. 3d shows the difference between calibrated FTIR measurements and IRMS values (FTIR-IRMS) against CO_2 mole fractions. Figure 3e–h show corresponding data for δ^{18}O-CO_2. The cross-sensitivity correction forces δ^{13}C-CO_2 and δ^{18}O-CO_2 onto a linear regression line (Fig. 3b and f), so that we can then apply a linear calibration. The large correction for δ^{18}O-CO_2 is most likely related to the systematic residual in the fitting of the spectra (Fig. 1a).

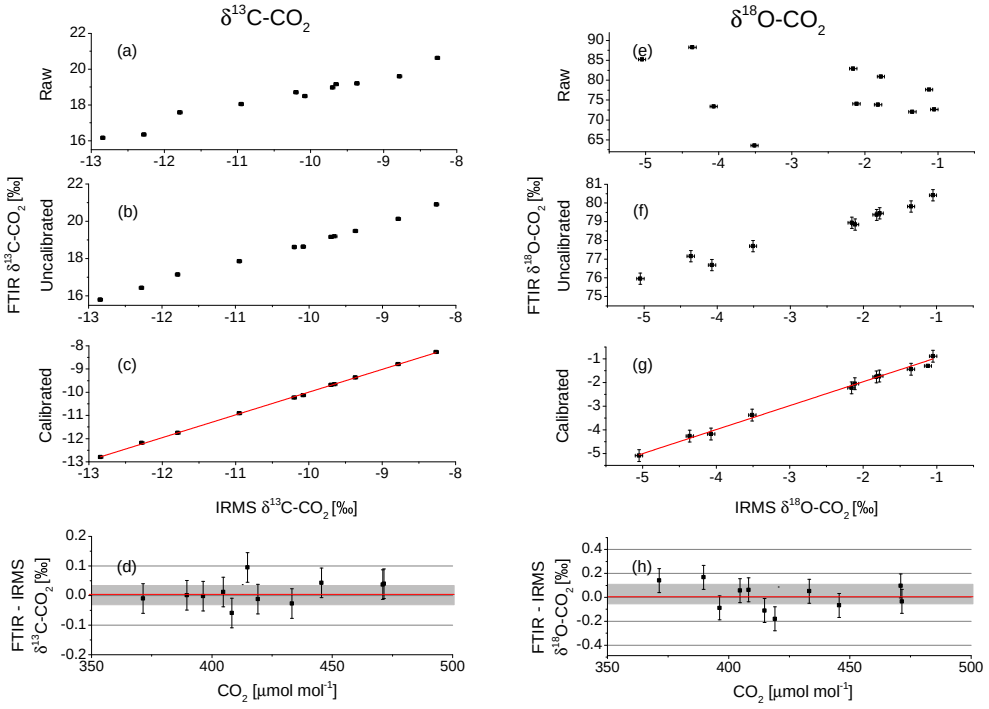

Figure 3. (a) Raw, **(b)** cross- and interspecies corrected (but still un-calibrated) and **(c)** calibrated δ^{13}C-CO_2 measurements and **(e)** raw, **(f)** cross- and interspecies corrected (but still un-calibrated); **(g)** calibrated δ^{18}O-CO_2 measurements of different target cylinders against the IRMS measurement of the same cylinders. Lowest panels: **(d)** calibrated FTIR δ^{13}C-CO_2 value minus reference value measured by the Heidelberg IRMS, **(h)** same as **(d)** for δ^{18}O-CO_2, both plotted versus the CO_2 mole fraction of the samples. The red lines in the lowest panels give the mean difference between the FTIR and the IRMS measurements. Grey areas illustrate the standard deviation of the differences.

2.2 Remarks on the calibration procedure

2.2.1 Using total CO_2 instead of $^{12}C^{16}O_2$ to calculate δ^{13}C-CO_2 and δ^{18}O-CO_2

As pointed out above, the precision of total CO_2 measurement in the 3600 cm^{-1} range is significantly higher ($\sim 50\,\%$) than that of $^{12}C^{16}O_2$ in the region of 2300 cm^{-1}, due to an optimum absorption strength and a lower temperature sensitivity. $^{12}C^{16}O_2$, $^{13}C^{16}O_2$ as well as $^{12}C^{16}O^{18}O$ absorb in this region, but the minor isotopologue absorptions are weak and are barely distinguishable. Thus, we calculate the raw δ^{13}C-CO_2 and δ^{18}O-CO_2 values using total CO_2 from the 3600 cm^{-1} region instead of $^{12}C^{16}O_2$. There is a small bias between measurements of CO_2 and$^{12}C^{16}O_2$, but as long as the isotopic composition of the sample is close to the isotopic composition of the reference standards, the bias in δ^{13}C-CO_2 and δ^{18}O-CO_2 is negligible ($< 0.03\,‰$ for δ^{13}C-CO_2 and $< 0.05\,‰$ for δ^{18}O-CO_2) after calibration (step 3). However, for strongly depleted cylinder gases, as may be the case for synthetic gas mixtures, the biases may become as large as 0.2 ‰. If necessary, the bias introduced by total CO_2 can be corrected iteratively using Eqs. (8) and (9) of Griffith et al. (2012):

$$^{12}C^{16}O_2 = \frac{CO_2}{X} \quad (4)$$

where X is an isotopic partition sum with a value very close to unity.

2.2.2 Direct isotopologue calibration

Griffith et al. (2012) described two methods for calibration of isotopic fractionations, either

a. the isotopologue amounts are calibrated independently and the isotopologue δ values calculated directly from the calibrated isotopologue amounts, or

b. the isotopologue δ values are calculated from raw measurements of the isotopologues and the calibration is carried through on the δ-values.

These methods were referred to as “absolute” and “empirical” calibration respectively by Griffith et al. (2012), but to avoid ambiguity we will refer to them here as (a) isotopologue calibration and (b) ratio or δ-calibration. The correction and calibration method described above and used in this work is the ratio calibration, (b). In principle, it is equally valid to use (direct) isotopologue calibration. In this case, we

correct the isotopologue amounts $^{16}O^{12}C^{16}O$, $^{16}O^{13}C^{16}O$ and $^{16}O^{12}C^{18}O$ (step 2), calibrate them individually (step 3) and finally compute δ^{18}O-CO_2 and δ^{13}C-CO_2 from the calibrated amounts, i.e.

$$\delta^{18}O - CO_{2,VPDB} = \left[\frac{\left(\frac{^{12}C^{18}O^{16}O}{^{12}C^{16}O^{16}O}\right)_{sample}}{\left(\frac{^{12}C^{18}O^{16}O}{^{12}C^{16}O^{16}O}\right)_{VPDB-CO_2}} - 1 \right] \cdot 1000\,‰ \quad (5)$$

with $(^{12}C^{18}O^{16}O/^{12}C^{16}O_2)_{VPDB-CO_2} = 0.0041767$ (Allison et al., 1995), which takes into account that CO_2 contains two oxygen atoms.

In principle, both methods should lead to the same results, but they are sensitive to errors in different ways (Griffith et al., 2012). In practice, we find they differ by about 0.11 ± 0.03 ‰ for δ^{13}C-CO_2 and by 0.08 ± 0.15 ‰ for δ^{18}O-CO_2 (mean $\pm$ standard deviation for a 2-month period in 2014). The discrepancy between both calibration methods is most likely due to small inaccuracies in interspecies interference corrections. The ratio calibration requires a large CO_2-interspecies interference correction over a large CO_2 range (see Fig. 2c). Only if the CO_2 interspecies interference correction is well determined can we obtain a reliable δ^{18}O-CO_2 value from the ratio method. For the independent isotopologue calibration, no explicit interspecies CO_2 correction is required, but a very accurate determination of all CO_2 isotopologue calibration equations is vital. The decision on which method to use should thus be based on which correction can be performed with higher accuracy. In this work, we have found for the Heidelberg spectrometer that the empirical calibration method better fits the Heidelberg IRMS values.

2.3 Direct cylinder comparison to mass spectrometric values

In order to check the FTIR calibration as well as the compatibility of the FTIR and the Heidelberg IRMS Finnigan MAT 252, we analysed measurements of different test cylinders in March and April 2014 on both instruments. The IRMS values are linked to the VPDB scale via three pure CO_2 reference gases (RM8562, RM8563 and RM8564). The FTIR reference cylinders were calibrated by the IRMS and thus the FTIR and the IRMS are on the same scale. For all cylinder measurements with the IRMS, we filled cylinder air into evacuated flasks from an intermediate transfer volume; we then analysed these flasks by both techniques like regular flask samples, since pressure regulator effects have often disturbed the IRMS analyses. The precision of the IRMS is about 0.02–0.03 ‰ for δ^{13}C-CO_2 and 0.05–0.1 ‰ for δ^{18}O-CO_2 (standard deviation of repeated flask measurements). Further, Wendeberg et al. (2013) have shown that the Heidelberg IRMS scale does not exhibit any significant scale contraction errors or errors through cross contamination between sample and standard measurements in the IRMS. For more details on the IRMS, see Neubert (1998). A two-sample t test reveals that, at the 0.01 significance level, the means of the FTIR and the IRMS measurements (Fig. 3d and h) for δ^{13}C-CO_2 and for δ^{18}O-CO_2 do not differ significantly and thus, are compatible.

3 Characterisation of δ^{18}O-CO_2 and δ^{13}C-CO_2 measurements with the Heidelberg FTIR

3.1 Allan deviation

We performed an Allan deviation repeatability test (Werle et al., 1993; Werle et al., 2011) on the FTIR system over 6 days from 17 September 2011 to 23 September 2011, with flowing sample supplied from a reference gas cylinder with a δ^{13}C-CO_2 value of about -10.1 ‰ and a δ^{18}O-CO_2 value of about -3.7 ‰. We used the Allan deviation as a measure for the repeatability (following JCGM, 2008) as shown in Fig. 4. Allan deviation is the standard deviation of the pairwise differences between adjacent measurements averaged over different averaging periods. In the absence of drift and with only white (random) noise, the Allan deviation will decrease with the square root of the averaging time. We found that the Allan deviations after 10 min were δ^{13}C-$CO_2 = \pm 0.03$ ‰ and δ^{18}O-$CO_2 = \pm 0.25$ ‰ (Fig. 4a and b). After 30 min, the Allan deviations decrease to δ^{13}C-$CO_2 = \pm 0.02$ ‰ and δ^{18}O-$CO_2 = \pm 0.15$ ‰. From 2 hours to up to 1 day, the Allan deviations stayed below about δ^{13}C-$CO_2 = \pm 0.02$ ‰ and δ^{18}O-$CO_2 = \pm 0.10$ ‰. No significant increase in Allan deviation could be observed within 1 day, since drifts on this time scale are small compared to the noise. Further, we can confirm that the frequency of smoothed working standard correction is adequate, since between daily working standard gas measurements the system remains stable within 0.02 ‰ for δ^{13}C-CO_2 and 0.10 ‰ for δ^{18}O-CO_2. In Heidelberg, a typical diurnal variation of δ^{18}O-CO_2 is of the order of 1 ‰ (see Sect. 4). Thus, the system is stable enough to resolve diurnal ambient δ^{18}O-CO_2 variations (see Sect. 4).

3.2 Intermediate measurement precision

We monitored the intermediate measurement precision (following JCGM, 2008) by measuring standard gases every day or week under reproducible conditions. The averaging time for each cylinder measurement was 9 min. We used the standard deviation of the 9 min cylinder gas averages to estimate the intermediate measurement precision of our instrumental set-up. For δ^{13}C-CO_2 and δ^{18}O-CO_2, we found that the intermediate measurement precision was 0.04 ‰ and 0.27 ‰, respectively for the period from December 2012 to October 2013 (see Fig. 5a and b). The Allan deviation at 9 min is very close to the standard deviation of the daily working cylinder measurements, which shows that for our system and laboratory conditions the repeatability dominates the intermediate measurement precision.

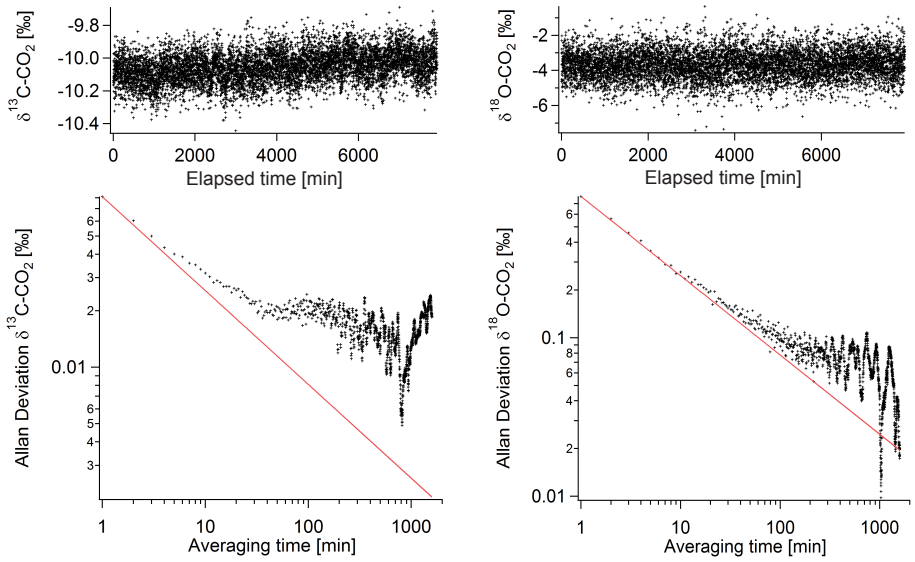

Figure 4. Allan deviation of δ^{13}C-CO_2 (left) and δ^{18}O-CO_2 (right) measured over the course of 6 days in September 2011 with the FTIR.

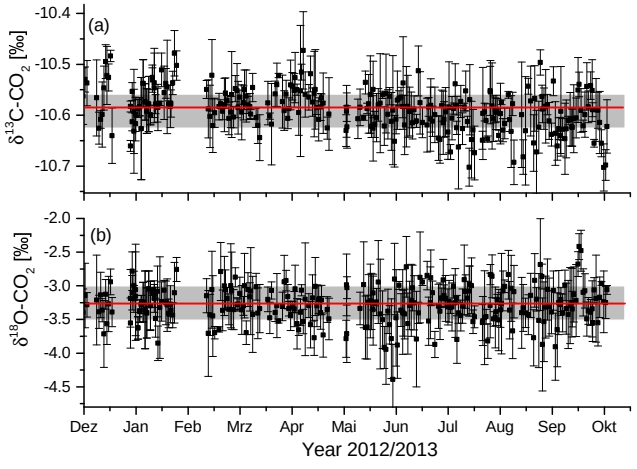

Figure 5. Repeated daily working gas measurements (9 min averages) depict an intermediate measurement precision of **(a)** ±0.04 ‰ for δ^{13}C-CO_2 and of **(b)** ±0.27 ‰ for δ^{18}O-CO_2 **(b)** for the period from December 2012 to October 2013. Red lines: mean values, grey areas: standard deviation.

Note that in our calibration procedure we now use the daily measured cylinder (working standard gas) in a final correction step (step 4) to account for sub-weekly variations of the instrument response. Since we only recognised the need to correct for this variability well after commencement of the measurements, we do not yet have a long-term record for a real surveillance cylinder. Therefore, Fig. 5 displays the working standard measurements without any sub-weekly smoothing applied, and thus gives an upper estimate of the intermediate measurement precision of real measurements where we apply step 4 of our calibration procedure in addition.

3.3 Compatibility of ambient air measurements

In the previous sections, we have evaluated the repeatability, as well as the intermediate measurement precision of the FTIR measurements. The results make us confident that the FTIR spectrometer is of sufficient precision and stability to resolve atmospheric signals, such as the diurnal variation of δ^{13}C-CO_2 and δ^{18}O-CO_2. Further, we have shown in Sect. 2.3 that the FTIR cylinder gas measurements are compatible to those of the Heidelberg IRMS. In order to show that not only the direct cylinder measurements, but also the ambient air measurements are compatible with the IRMS analyses, we compared in situ ambient air samples, which we measured with both instruments.

For this purpose, an automated flask sampler (Neubert et al., 2004) collected dried (dew point −40 °C) ambient air from the same intake line as the FTIR into 2.5 litre glass flasks. Every flask was flushed with a flow rate of about 1.1 SLPM for 2 h and then pressurised to 2000 hPa absolute pressure and closed. Then the automated flask sampler opened, flushed and filled the next flask to 2000 hPa. Pressurising the flasks took about 5 min. With this procedure, we were able to capture a diurnal isotopic profile with a 2-hourly resolution in the flasks, which could be analysed by mass spectrometry. We then compared these values to the continuous values measured by the FTIR spectrometer; the results are shown in Fig. 6. We used 9 min averaged values from the FTIR spectrometer to compare them to the flask results to account for atmospheric variability and to minimise differences due to lack of temporal synchronisation between the event sampler and the FTIR, and to reduce the noise on the FTIR measurement. We found that the mean residual and standard error is 0.01 ± 0.02 ‰ for δ^{13}C-CO_2 and 0.08 ± 0.14 ‰ for δ^{18}O-

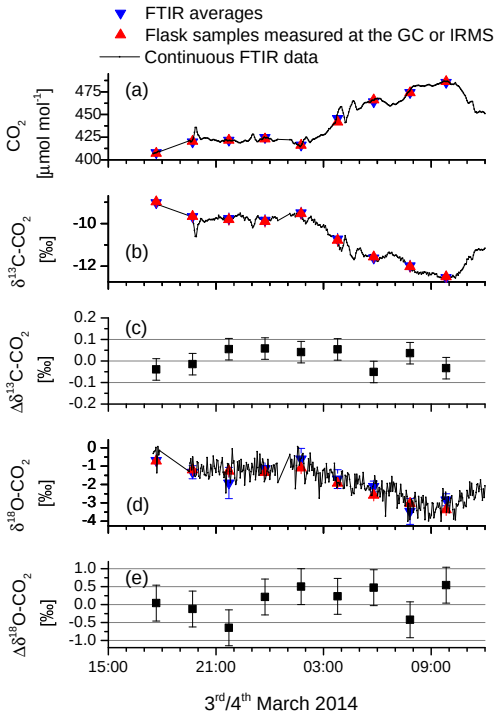

Figure 6. Diurnal cycle event sampled on the 3–4 March 2014 at the Institut für Umweltphysik in Heidelberg. Red: GC concentration (in case of CO_2) or IRMS isotopologue value (in case of isotopologues) of flasks samples; blue: 9 min averaged values from FTIR; black: continuous 3 min values from the FTIR. **(a)** CO_2 mole fraction; **(b)** δ^{13}C-CO_2 value; **(c)** residual of 9 min average δ^{13}C-CO_2 FTIR and IRMS measurement (FTIR - IRMS); **(d)** δ^{18}O-CO_2 value; **(e)** residual of 9 min averaged δ^{18}O-CO_2 FTIR and IRMS measurement (FTIR – IRMS). All error bars on the (blue) averaged FTIR data are the standard deviation during the 9 min of averaging time. The error bars on the (red) IRMS values show the typical intermediate measurement precision of our IRMS measurements. The residual (FTIR-IRMS) has an error bar, which combines the IRMS uncertainty and the FTIR uncertainty and the variability of atmospheric signal during the flask filling time.

CO_2 (FTIR – IRMS). We tested the compatibility between the FTIR and the IRMS ambient air measurements with a two-sample t test and found that at the 0.01 significance level, the means of the FTIR and the IRMS measurements in ambient air do not differ from each other for δ^{13}C-CO_2 or for δ^{18}O-CO_2. Note, that the standard deviation of the differences between the FTIR and the IRMS is 0.05 ‰ for δ^{13}C-CO_2 and 0.42 ‰ for δ^{18}O-CO_2 and with that the standard deviation for δ^{18}O-CO_2 differences is higher than expected from the combined Allan deviation (0.25 ‰ for 9 min averages) and the uncertainty of the IRMS measurement (ca. 0.05–0.1 ‰).

The slightly larger variability in δ^{18}O-CO_2 ambient air comparison than in cylinder gas comparisons (Sect. 2.3) reflects the fact that there are more contributions to the difference between the FTIR and the IRMS flask measurement. There are the storage effect of the flasks themselves, which could be slightly wet and thus alter the δ^{18}O value of the CO_2 in the flask, or some other possible interference of the automated flask sampler (i.e. varying integration time due to flow and pressure variations).

4 Example period of continuous trace gas and stable isotopologue measurements in Heidelberg

In this section, we illustrate how we might potentially use a highly resolved δ^{18}O-CO_2 record at a typical European monitoring station, such as Heidelberg, in order to disentangle regional scale carbon exchange processes. Note, however, that for a quantitative evaluation, we would require explicit information on local CO_2 source signatures and on the exchanging water reservoirs. We look here at two very different periods in which the FTIR measured δ^{18}O-CO_2 along with δ^{13}C-CO_2, total CO_2 and CO in Heidelberg (see Fig. 7).

In order to interpret the atmospheric δ^{18}O-CO_2 variation, we must estimate the isotopic signature or discrimination of the processes influencing the isotopic content. The Heidelberg catchment area is typical of many European urban areas with the most important CO_2 fluxes associated with plant photosynthesis, leaf and soil respiration, as well as fossil fuel burning. In the greater catchment area, discrimination during photosynthesis tends to enrich atmospheric CO_2 with respect to ^{13}C and ^{18}O (Cuntz et al., 2003b). Typical mean δ^{13}C fractionation relative to the atmosphere during photosynthesis is about – (2–8) ‰ for C4 plants and about – (12–20) ‰ for C3 plants (Mook, 1994). As a first approximation, the $^{13}CO_2$ / $^{12}CO_2$ ratio captured during photosynthesis is released during respiration, which leads to an overall depletion of the atmospheric $^{13}CO_2$ / $^{12}CO_2$ ratio. In addition, ^{18}O discrimination during respiration tends to deplete the atmosphere in its δ^{18}O-CO_2 value. Neubert (1998) measured the isotopic composition of soil-respired CO_2 in the surroundings of Heidelberg and found values of δ^{18}O-$CO_{2,\mathrm{VPDB}} \approx -10$ ‰ with a tendency of slightly more depleted values in winter (−15 ‰) than in summer (−5 ‰) and δ^{13}C-$CO_{2,\mathrm{VPDB}} \approx -25$ ‰. For the discrimination during photosynthesis, typical mean values for the central European continent are between 0 and +20 ‰ for ^{18}O (Farquhar et al., 1993; Cuntz et al., 2003b). Further, the invasion flux will influence the apparent soil respiration signature (Tans, 1998; Miller et al., 1999), but we cannot quantify the magnitude of this effect for our catchment area without intensive sampling and isotopic soil flux modelling. Therefore, we only consider the invasion flux in a sense that a larger range must be attributed to the signature of the apparent soil respiration flux when qualitatively discussing our atmospheric δ^{18}O-CO_2 records here.

For the isotopic signature of fossil fuels, most studies assume a common δ^{18}O fossil fuel signature of δ^{18}O-$CO_{2,\mathrm{VPDB}} \approx -17$ ‰, corresponding to the ambient oxy-

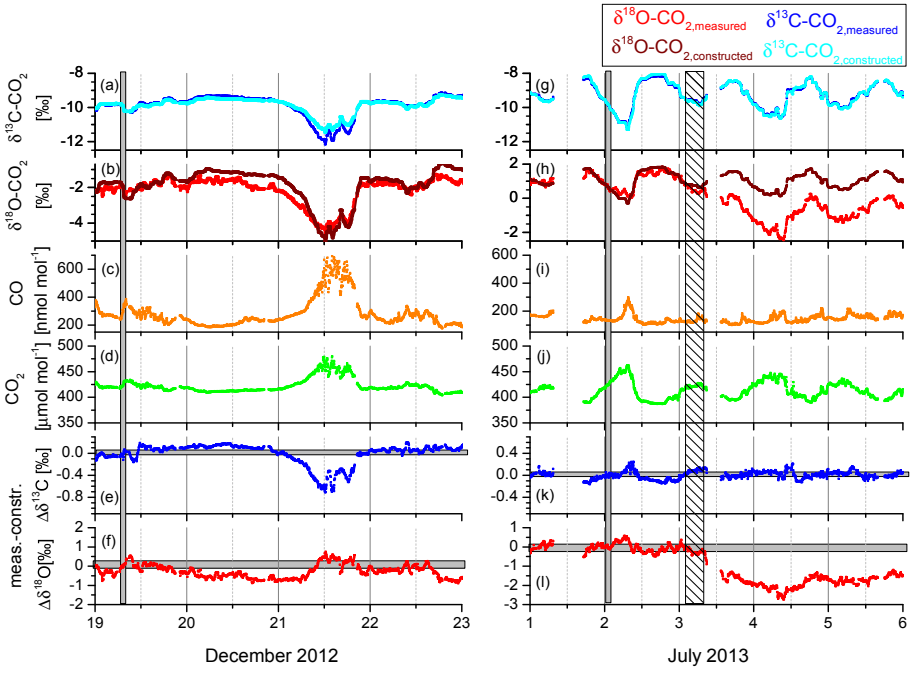

Figure 7. Trace gas records in winter (left panel) and summer (right panel) in Heidelberg. **(a)** and **(g)** show the measured (dark blue) and artificially constructed (light blue) δ^{13}C-CO_2 value, **(b)** and **(h)** the measured (red) and artificially constructed (burgundy) δ^{18}O-CO_2 value, **(c)** and **(i)** the measured CO value, **(d)** and **(j)** the measured CO_2 value. Panels **(e)** and **(k)** give the difference between the measured and constructed δ^{13}C-CO_2 value with a mean isotopic source signature of δ^{13}C-$CO_{2,\mathrm{VPDB}} \approx -25$ ‰ in the wintertime and δ^{13}C-$CO_{2,\mathrm{VPDB}} \approx -27$ ‰ in the summertime. Panels **(f)** and **(l)** give the difference between the measured and constructed δ^{18}O-CO_2 value with a mean isotopic signature of δ^{18}O-$CO_{2,\mathrm{VPDB}} \approx -28$ ‰ in the wintertime and δ^{18}O-$CO_{2,\mathrm{VPDB}} \approx -12$ ‰ in the summertime. Grey vertical bars indicate the "reference periods", in which the isotopic source signature for artificially constructed δ^{13}C-CO_2 and δ^{18}O-CO_2 was determined from Keeling plots of about 20 individual atmospheric 3 min average measurements. The dashed vertical bar in the right panel shows a period of high precipitation. Grey horizontal bars in **(f)** and **(l)** mark the 1σ-uncertainty of the isotope measurements.

gen isotopic signature, but incomplete combustion can lead to a range of different isotopic signatures. The ^{18}O signature of fossil fuel emissions varies from about δ^{18}O-$CO_{2,\mathrm{VPDB}} \approx -11$ to -40 ‰ (Schumacher et al., 2011). Traffic exhausts tend to be less depleted in ^{18}O relative to other fossil fuel CO_2 emissions (δ^{18}O-$CO_{2,\mathrm{VPDB}} \approx -15$ ‰), followed by natural gas burning (δ^{18}O-$CO_{2,\mathrm{VPDB}} \approx -28$ ‰). Combustion of coal, on the other hand, leads to a δ^{18}O-CO_2 value of about -38 ‰ (Schumacher et al., 2011). To our knowledge, the potential range of these values is not well known. For δ^{13}C, typical signatures are δ^{13}C-$CO_{2,\mathrm{VPDB}} \approx -29$ ‰ for traffic exhausts, -25 ‰ for coal combustion and -39 ‰ for natural gas emissions (Widory and Javoy, 2003; Kaul, 2007). With these examples of isotopic signatures, we can now look at our atmospheric CO_2 records that show values of δ^{13}C-CO_2 between δ^{13}C-$CO_{2,\mathrm{VPDB}} \approx -8$ and -12 ‰, while δ^{18}O-CO_2 varies between δ^{18}O-$CO_{2,\mathrm{VPDB}} \approx -2$ to -4 ‰ in winter and 0 to -2 ‰ in summer (Fig. 7).

Since all CO_2 sources with a negative isotopic signature relative to atmospheric CO_2 lead to δ^{13}C-CO_2 or δ^{18}O-CO_2 depletion, a differentiation between different depleting sources is difficult. Therefore we used the following approach: We first constructed an artificial δ^{13}C-CO_2 and δ^{18}O-CO_2 record using the slope (a_{ref}) and offset (b_{ref}) of so-called "Keeling plots" (Keeling, 1958), determined from measured atmospheric δ- and CO_2 concentration values in an exemplary and short nighttime reference period (grey bars in Fig. 7) according to:

$$\delta_{\mathrm{meas}} = a_{\mathrm{ref}} \cdot \frac{1}{\mathrm{CO_2}} + b_{\mathrm{ref}} \tag{6}$$

Note that in the nighttime reference periods, for which the reference slope and offsets were calculated, we can neglect photosynthetic sinks. Therefore, we can interpret the δ^{13}C source signature of the reference period as the flux-weighted average of all sources (Miller and Tans, 2003). We then applied the parameters (a_{ref} and b_{ref}) from the reference period to the entire CO_2 record to calculate artificially constructed $\delta^{13}C_{\mathrm{constr}}$ and $\delta^{18}O_{\mathrm{constr}}$ values:

$$\delta_{\mathrm{constr(t)}} = a_{\mathrm{ref}} \cdot \frac{1}{\mathrm{CO_2(t)}} + b_{\mathrm{ref}}, \tag{7}$$

Fig. 7a, b, g and h show the constructed δ^{13}C-CO_2 and δ^{18}O-CO_2 records in burgundy and light blue. During the ref-

erence period in which the Keeling plot slopes and offsets were derived, the Keeling plot had a high correlation coefficient ($r^2 > 0.85$) and showed an isotopic ^{13}C and ^{18}O source signature that was typical for the respective season (source δ^{13}C-$CO_2 \approx -25$ ‰ in the winter and -27 ‰ in the summer period, δ^{18}O-$CO_2 \approx -28$ ‰ in the winter and -12 ‰ in the summer period). To identify influences from enriching or depleting sources and sinks relative to those in the reference period, we then calculated the difference between the measured and the artificially constructed (Eq. 6) δ^{13}C-CO_2 and δ^{18}O-CO_2 record (Fig. 7e, k, f and l):

$$\Delta\delta(t) = \delta_{meas}(t) - \delta_{constr}(t). \quad (8)$$

Negative $\Delta\delta$ values occur in periods when the apparent sources are more depleted than in the reference period and positive values occur when apparent sources are more enriched than in the reference period. During photosynthetic CO_2 uptake, the equilibration of back-diffusing CO_2 with enriched leaf water leads to an enrichment of atmospheric δ^{18}O-CO_2 and thus to positive $\Delta\delta^{18}$O values. We now have a tool that allows differentiation between more and less depleted fluxes relative to the reference period.

In the wintertime, relative fossil fuel contributions in the Heidelberg catchment area are higher than in the summertime (Levin et al., 2003). Fossil fuel CO_2 emissions lead to high concentration of CO_2 (Fig. 7d) and deplete atmospheric CO_2 in its heavy isotopes ^{13}C and ^{18}O (original measurements: dark blue and red in Fig. 7a, b). During incomplete combustion of fossil fuels, CO (Fig. 7c) is often emitted as well. A typical example of a pollution event is shown in Fig. 7 (left panel) on 21 December 2012. The difference between the measured and artificially constructed δ^{13}C-CO_2 (Fig. 7e) decreases rapidly on 21 December. Environmental parameters such as relative humidity, global radiation and temperature (not shown here) remain constant during the event, but low wind speed leads to an atmospheric inversion and, accompanied with a slight change of wind direction, to a more local source (mix), which is more depleted in ^{13}C than during the reference period ($\delta^{13}C_{ref} = -25$ ‰). The strong influence of a more ^{13}C depleted source mix points towards a high contribution from fossil fuel sources, including domestic heating (natural gas). At the same time, the isotopic signature of δ^{18}O-CO_2 is very close to the isotopic signature during the reference period (-28 ‰) and increases during the pollution event. The different behaviour of δ^{13}C and δ^{18}O in CO_2 points towards a larger influence from traffic or natural gas combustion, as both sources are slightly more enriched in ^{18}O, but less enriched in ^{13}C with respect to coal-fired combustion (Schumacher et al., 2011). One can see that the fact that different fossil fuel types influence both stable isotopes ^{13}C and ^{18}O in CO_2 in a different way can potentially be used to differentiate between different emission groups in situations when biogenic fluxes are low (i.e. in winter). However, for a quantitative analysis we must know the exact isotopic signatures of all fluxes in the area of influences.

In the summertime, we expect biosphere fluxes to be much larger than during winter and at the same time fossil fuel (especially residential heating) emissions to be smaller than in winter. In fact, we do not find large deviations in $\delta^{13}CO_2$ from those determined in the reference period (-27 ‰), pointing towards a relatively constant mixture of biogenic and fossil fuel emissions. On the other hand, the measured δ^{18}O-CO_2 decreased rapidly on 3 July, compared to the reference period with a source isotopic signature of ≈ -12 ‰. This decrease is not accompanied by changes of any other tracer, such as CO, $\delta^{13}CO_2$ or CO_2, and also not by drastic changes of environmental parameters such as relative humidity, temperature or wind speed (not shown here). A possible explanation for the decrease is a change in the hydrological conditions. After 4 dry days, a sudden heavy rain occurred in Heidelberg on 3 July (see dashed bar in Fig. 7, right panel). The rainfall replenished the water reservoirs with an ^{18}O-depleted signature (Daansgard et al., 1964) and equilibration between the soil and leaf water reservoirs and CO_2 most probably caused the atmospheric δ^{18}O-CO_2 to become depleted relative to the reference period. This example illustrates the close coupling between δ^{18}O in the water and carbon cycle. It is thus crucial to study also the hydrological conditions, such as precipitation and its isotopic signature, in order to quantitatively use the δ^{18}O-CO_2 records for carbon cycle research.

5 Discussion

5.1 Instrumental performance

The main scope of this work was to ascertain whether the FTIR analyser is capable of measuring δ^{18}O-CO_2 in the atmosphere and if so, to assess how well it performs. We have seen that the FTIR succeeds in measuring atmospheric δ^{18}O-CO_2 with a high repeatability (Allan deviation after 1 day: 0.1 ‰) and good intermediate measurement precision (δ^{18}O-$CO_2 = 0.27$ ‰ for daily repeated working standard gas measurements on 9 min averages over 10 months). We were also able to confirm a good compatibility to the IRMS. Some optimisation, concerning the calibration, the fitted spectral windows and the theoretical spectrum modelling could lead to improved results. However, the current performance of the spectrometer suffices to quantify typical diurnal and synoptic variations at an urban site, which is an important step towards quantification of gross biospheric fluxes using FTIR-based δ^{18}O-CO_2 measurements.

5.2 Quantitative interpretation of continuous δ^{13}C-CO_2 and δ^{18}O-CO_2 record

We further investigated which insight may be gained from continuous isotopologue records at an urban site. For δ^{13}C, the different carbon sources and sinks are relatively well understood, but for δ^{18}O, high temporal variability of the res-

piratory and photosynthetic fluxes (due to a strong variation of environmental parameters such as precipitation, temperature and humidity) makes it difficult to separate the different CO_2 fluxes. For our qualitative study, we could use observations from Neubert (1998) in the catchment area of Heidelberg, as well as globally resolved model data for assimilation isofluxes from Cuntz et al. (2003b). However, for a quantitative apportionment of the CO_2 fluxes at a high temporal resolution, sampling of the isotopic content of precipitation, soil respiration and foliage gas exchange in the catchment area will be necessary with similarly high temporal resolution (Stern et al., 1999; Langendörfer et al., 2002). Further, isotope soil-atmosphere flux models are required to quantify the effect of this process at the measurement site. All of these unknowns largely limit current applicability of our new continuous isotope measurements. Future sophisticated regional models of the water and the carbon cycle may, however, be able to fully exploit the wealth of new information now available.

6 Summary and conclusion

The analysis of δ^{18}O in CO_2 using FTIR spectroscopy is novel. We evaluated the measurements of ^{18}O in CO_2 using the FTIR with respect to repeatability, intermediate measurement precision and compatibility. The Allan deviation test showed that the instrument measures δ^{18}O-CO_2 with good stability over the course of a day (the frequency of the working standard measurement) to within 0.1 ‰. Averages of 9 min show a standard deviation of about 0.25 ‰, which is in agreement with the intermediate measurement precision based on daily working standard gas measurements.

Evaluation of diurnal ambient air variations is therefore possible using, for example, 30 min averages. The high temporal resolution of the FTIR measurement is a major advantage over the IRMS analyses. Even though the FTIR precision does not reach the WMO inter-laboratory compatibility targets (WMO, 2012), a number of interesting scientific applications seem possible using FTIR spectroscopy. In particular, investigation of the processes that govern the δ^{18}O-CO_2 variability of atmospheric CO_2 on the regional scale seem very promising if comprehensive knowledge on the isotopic signature of different CO_2 sources and sinks, as well as of the influencing water reservoirs, is available.

Acknowledgements. We thank Geoff Toon, Frank Hase and Joseph Mendonca for valuable discussions on molecular line shapes spectra and for fitting our spectra with different line shape models. Four anonymous reviewers are gratefully acknowledged for their valuable comments, which helped to improve our manuscript. This work has been funded by the InGOS EU project (284274). We further acknowledge the financial support given by Deutsche Forschungsgemeinschaft and Ruprecht-Karls-Universität Heidelberg within the funding program Open Access Publishing.

Edited by: G. Phillips

References

Allison, C., Francey, R., and Meijer, H.: Recommendations for the reporting of stable isotope measurements for carbon and oxygen in CO_2 gas, Reference and intercomparison materials for stable isotopes of light element, IAEA-TECDO, 155–162, 1995.

Bowling, D. R., McDowell, N. G., Welker, J. M., Bind, B. J., Law, B.E., and Ehleringer, J. R.: Oxygen isotope content of CO_2 in nocturnal ecosystem respiration: 1. Observations in forests along a precipitation transect in Oregon, USA, Global Biogeochem. Cy., 17, 1120, doi:10.1029/2003GB002081, 2003.

Buenning, N., Noone, D., Randerson, J., Riley, W. J., and Still, C.: The response of the $^{18}O/^{16}O$ composition of atmospheric CO_2 to changes in environmental conditions, J. Geophys. Res.-Biogeosci., 119, 55–79, doi:10.1002/2013JG002312, 2014.

Cambaliza, M. O. L.: Measurement of forest ecosystem-atmosphere exchange of δ^{13}C-CO_2 using Fourier Transform Infrared spectroscopy and disjunct eddy covariance, Dissertation, Washington State University, Department of Civil and Environmental Engineering, USA, 2010.

Ciais, P., Tans, P. P., White, J. W. C., Trolier, M., Francey, R. J., Berry, J. A., Randall, D. R., Sellers, P. J., Collatz, J. G., and Schimel, D. S.: Partitioning of ocean and land uptake of CO_2 as inferred by δ^{13}C measurements from the NOAA Climate Monitoring and Diagnostics Laboratory Global Air Sampling Network, J. Geophys. Res., 100, 5051–5070, doi:10.1029/94JD02847, 1995.

Ciais, P., Denning, A. S., Tans, P. P., and Berry, J. A.: A three-dimensional synthesis study of δ^{18}O in atmospheric CO_2 1.surface fluxes, J. Geophys. Res., 102, 5857–5872, doi:10.1029/96JD02360, 1997.

Coplen, T. B.: Guidelines and recommended terms for expression of stable-isotope-ratio and gas-ratio measurement results. Rapid Commun. Mass Spectrom., 25, 2538–2560, doi:10.1002/rcm.5129, 2011.

Cuntz, M., Ciais, P., Hoffmann, G., and Knorr, W.: A comprehensive global three-dimensional model of δ^{18}O in atmospheric CO_2: 1. Validation of surface processes, J. Geophys. Res., 108, 4527, doi:10.1029/2002jd003153, 2003a.

Cuntz, M., Ciais, P., Hoffmann, G., Allison, C. E., Francey, R. J., Knorr, W., Tans, P. P., White, J. W. C., and Levin, I.: A comprehensive global three-dimensional model of δ^{18}O in atmospheric CO_2: 2. Mapping the atmospheric signal, J. Geophys. Res., 108, 4528, doi:10.1029/2002JD003154, 2003b.

Daansgard, W.: Stable isotopes in precipitation, Tellus, 16, 436–468, doi:10.1111/j.2153-3490.1964.tb00181.x, 1964.

Esler, M. B., Griffith, D. W. T, Wilson, S. R., and Steele, L. P.: Precision trace gas analysis by FT-IR Spectroscopy. 2. The $^{13}C/^{12}C$ Isotope Ratio of CO_2, Anal. Chem, 72, 216–221, 2000.

Farquhar, G. D., Lloyd, J., Taylor, J. A., Flanagan, L. B., Syvertsen, J. P., Hubick, K. T., Wong, S. C., and Ehleringer, J. R.: Vegetation effects on the isotope composition of oxygen in atmospheric CO_2, Nature, 363, 439–443, doi:10.1038/363439a0, 1993.

Flanagan, L. B., Brooks, J. R., Varney, G. T., and Ehleringer, J. R.: Discrimination against $C^{18}O^{16}O$ during photosynthesis and the

oxygen isotope ratio respired CO_2 in boreal forest ecosystems, Global Biogeochem. Cy., 11, 83–98, 1997.

Francey, R. J. and Tans, P. P.: Latitudinal variation in oxygen-18 of atmospheric CO_2, Nature, 327, 495–497, doi:10.1038/327495a0, 1987.

Gillon, J. and Yakir, D.: Influence of carbonic anhydrase activity in terrestrial vegetation on the ^{18}O content of atmospheric CO_2, Science, 291, 2584–2587, doi:10.1126/science.1056374, 2001.

Griffith, D. W. T.: Synthetic calibration and quantitative analysis of gas phase infrared spectra, Appl. Spectrosc., 50, 59–70, 1996.

Griffith, D. W. T., Jamie, I. M., and Meyers, R. A. (Eds.): Fourier Transform Infrared Spectrometry in Atmospheric and Trace Gas Analysis, Encyclopedia of Analytical Chemistry, Wiley, Chichester, 2000.

Griffith, D. W. T., Deutscher, N. M., Caldow, C., Kettlewell, G., Riggenbach, M., and Hammer, S.: A Fourier transform infrared trace gas and isotope analyser for atmospheric applications, Atmos. Meas. Tech., 5, 2481–2498, doi:10.5194/amt-5-2481-2012, 2012.

Hammer, S., Griffith, D. W. T., Konrad, G., Vardag, S., Caldow, C., and Levin, I.: Assessment of a multi-species in situ FTIR for precise atmospheric greenhouse gas observations, Atmos. Meas. Tech., 6, 1153-1170, doi:10.5194/amt-6-1153-2013, 2013a.

Hammer, S., Konrad, G., Vermeulen, A. T., Laurent, O., Delmotte, M., Jordan, A., Hazan, L., Conil, S., and Levin, I.: Feasibility study of using a "travelling" CO_2 and CH_4 instrument to validate continuous in situ measurement stations, Atmos. Meas. Tech., 6, 1201–1216, doi:10.5194/amt-6-1201-2013, 2013b.

Hase, F., Drouin, B. J., Roehl, C. M., Toon, G. C., Wennberg, P. O., Wunch, D., Blumenstock, T., Desmet, F., Feist, D. G., Heikkinen, P., De Mazière, M., Rettinger, M., Robinson, J., Schneider, M., Sherlock, V., Sussmann, R., Té, Y., Warneke, T., and Weinzierl, C.: Calibration of sealed HCl cells used for TCCON instrumental line shape monitoring, Atmos. Meas. Tech., 6, 3527–3537, doi:10.5194/amt-6-3527-2013, 2013.

Hesterberg, R. and Siegenthaler, U.: Production and stable isotopic composition of CO_2 in a soil near Bern, Switzerland. Tellus B, 43, 197–205, doi:10.1034/j.1600-0889.1991.00013.x, 1991.

JCGM: Joint Committee for Guides in Metrology: International vocabulary of metrology – basic and general concepts and associated terms (VIM), 3rd Edn., 2008.

Kaul, M.: Isotopenverhältnisse im atmosphärischem Kohlendioxid und seine Quellen im Raum Heidelberg, Staatsexamen thesis, Universität Heidelberg, Heidelberg, Germany, 2007.

Keeling, C. D.: The concentration and isotopic abundance of atmospheric carbon dioxide in rural areas, Geochim. Cosmochim. Ac. 13, 322–334, 1958.

Keeling, C. D., Bacastow, R. B., Carter, A. F., Piper, S. C., Whorf, T. P., Heimann, M., Mook, W. G. and Roeloffzen, H.: A three-dimensional model of atmospheric CO_2 transport based on observed winds: 1. Analysis of observational data, Aspects of Climate Variability in the Pacific and the Western Americas, edited by: Peterson, D. H., Vol. 55, American Geophysical Union, Washington, D. C., 165–236, 1989.

Langendörfer, U., Cuntz, M., Ciais, P., Peylin, P., Bariac, T., Milyukova, I., Kolle, O., Naegler, T., and Levin, I.: Modelling of biospheric CO_2 gross fluxes via oxygen isotopes in a spruce forest canopy: a ^{222}Rn calibrated box model approach. Tellus B, 54, 476–496, doi:10.1034/j.1600-0889.2002.01345.x, 2002.

Levin, I., Kromer, B., Schmidt, M., and Sartorius, H.: A novel approach for independent budgeting of fossil fuel CO_2 over Europe by $^{14}CO_2$ observations, Geophys. Res. Lett., 30, 2194, doi:10.1029/2003GL018477, 2003.

Miller, J. B. and Tans, P. P.: Calculating isotopic fractionation from atmospheric measurements at various scales, Tellus B, 55, 207–214. doi:10.1034/j.1600-0889.2003.00020.x, 2003.

Miller, J. B., Yakir, D., White, J. W. C., and Tans, P. P.: Measurement of $^{18}O/^{16}O$ in the soil-atmosphere CO_2 flux, Global Biogeochem. Cy., 13, 761–774, doi:10.1029/1999GB900028, 1999.

Mohn, J., Zeeman, M. J., Werner, R. A., Eugster, and W., Emmenegger, L.: Continuous field measurements of $\delta^{13}C - CO_2$ and trace gases by FTIR spectroscopy, Isotopes Environ. Health Stud., 44, 241–251, 2008.

Mook, W.: Environmental isotopes in the hydrological cycle – Principles and applications, Introductory course on Isotope Hydrology, Department of Hydrogeology and Geographical Hyrdology, 1994.

Neubert, R.: Measurement of stable isotopomers of atmospheric carbon dioxide, PhD thesis, University of Heidelberg, Heidelberg, Germany, 1998.

Neubert, R. E. M., Spijkervet, L. L., Schut, J. K., Been, H. A., and Meijer, H. A. J.: A computer-controlled continuous air drying and flask sampling system, J. Atmos. Ocean. Technol., 21, 651–659, 2004.

Ngo, N. H., Lisak, D., Tran, H., and Hartmann, J.-M.: An isolated lineshape model to go beyond the Voigt profile in spectroscopic databases and radiative transfer codes. J. Quant. Spectrosc. Ra., 129, 89–100, 2013.

Pataki, D. E., Bowling, D. R., and Ehleringer, J. R.: Seasonal cycle of carbon dioxide and its isotopic composition in an urban atmosphere: Anthropogenic and biogenic effects, J. Geophys. Res., 108, 4735, doi:10.1029/2003JD003865, 2003.

Rothman, L. S., Jacquemart, D., Barbe, A., Benner, D. C., Birk, M., Brown, L. R., Carleer, M. R., C. Chaucerian, J., Chance, K., Dana, V., Devi, V. M., Flaud, J.-M., Gamache, R. R., Goldman, A., Hartmann, J.-M., Jucks, K. W., Maki, A. G., Mandin, J.-Y., Massie, S. T., Orphali, J., Perrin, A., Rinsland, C. P., Smith, M. A. H., Tennyson, J., Tolchenov, R. N., Toth, R. A., Auwera, J. V., Varanasi, P., and Wagner, G.: The HITRAN 2004 molecular spectroscopic database, J. Quant. Spectrosc. Ra., 96, 139–204, doi:10.1016/j.jqsrt.2004.10.008, 2005.

Schumacher, M., Werner, R. A., Meijer, H. A. J., Jansen, H. G., Brand, W. A., Geilmann, H., and Neubert, R. E. M.: Oxygen isotopic signature of CO_2 from combustion processes, Atmos. Chem. Phys., 11, 1473–1490, doi:10.5194/acp-11-1473-2011, 2011.

Seibt, U., Wingate, L., Lloyd, J., and Berry, J. A.: Diurnally variable $\delta^{18}O$ signatures of soil CO_2 fluxes indicate carbonic anhydrase activity in a forest soil, J. Geophys. Res., 111, G04005, doi:10.1029/2006JG000177, 2006.

Stern, L., Baisden, W. T., and Amundson, R.: Processes controlling the oxygen isotopic ratio of soil CO_2: analytical and numerical modelling, Geochim Cosmochim. Ac. 63, 799–814, 1999.

Still, C. J., Riley, W. J., Biraud, S. C., Noone, D. C., Buenning, N. H., Randerson, J. T., Tom, M. S., Welker, J., White, J .W. C., Vachon, R., Farquhar, G. D., and Berry, J. A.: Influence of clouds and diffuse radiation on ecosystem-atmosphere

CO_2 and $CO^{18}O$ exchanges, J. Geophys. Res., 114, G01018, doi:10.1029/2007JG000675, 2009.

Sturm, P., Tuzson, B., Henne, S., and Emmenegger, L.: Tracking isotopic signatures of CO_2 at the high altitude site Jungfraujoch with laser spectroscopy: analytical improvements and representative results, Atmos. Meas. Tech., 6, 1659–1671, doi:10.5194/amt-6-1659-2013, 2013.

Tans, P. P.: Oxygen isotopic equilibrium between carbon dioxide and water in soils. Tellus B, 50, 163–178, doi:10.1034/j.1600-0889.1998.t01-1-00004.x, 1998.

Tans, P. P. and Bolin, B. (Eds.): $^{13}C/^{12}C$ of industrial CO_2, Carbon Cycle Modelling, Scope Ser., 16, 127–129, 1981.

Tuzson, B., Henne, S., Brunner, D., Steinbacher, M., Mohn, J., Buchmann, B., and Emmenegger, L.: Continuous isotopic composition measurements of tropospheric CO_2 at Jungfraujoch (3580 m a.s.l.), Switzerland: real-time observation of regional pollution events, Atmos. Chem. Phys., 11, 1685–1696, doi:10.5194/acp-11-1685-2011, 2011.

Vardag, S. N., Hammer, S., O'Doherty, S., Spain, T. G., Wastine, B., Jordan, A., and Levin, I.: Comparisons of continuous atmospheric CH_4, CO_2 and N_2O measurements – results from a travelling instrument campaign at Mace Head, Atmos. Chem. Phys., 14, 8403–8418, doi:10.5194/acp-14-8403-2014, 2014.

Welp, L. R., Keeling, R. F., Meijer, H. A., Bollenbacher, A. F., Piper, S. C., Yoshimura, K., Francey, R. J., Allison, C. E., and Wahlen, M.: Interannual variability in the oxygen isotopes of atmospheric CO_2 driven by El Niño, Nature, 477, 579–582, 2011.

Wendeberg, M., Richter, J. M., Rothe, M., and Brand, W. A.: Jena Reference Air Set (JRAS): a multi-point scale anchor for isotope measurements of CO_2 in air, Atmos. Meas. Tech., 6, 817–822, doi:10.5194/amt-6-817-2013, 2013.

Werle, P. O., Mücke, R., and Slemr, F.: The limits of signal averaging in atmospheric trace-gas monitoring by tunable diode-laser absorption spectroscopy (TDLAS), Appl. Phys. B, 57.2, 131–139, 1993.

Werle, P.: Accuracy and precision of laser spectrometers for trace gas sensing in the presence of optical fringes and atmospheric turbulence, Appl. Phys. B, 10, 251–253, 2011.

Widory, D. and Javoy, M.: The carbon isotope composition of atmospheric CO_2 in Paris, Earth Planet. Sci. Lett., 215, 289–298, 2003.

Wingate, L., Seibt, U., Maseyk, K., Ogée, J., Almeida, P., Yakir, D., Pereira, J. S., and Menunccini, M.: Evaporation and carbonic anhydrase activity recorded in oxygen isotope signatures of net CO_2 fluxes from a Mediterranean soil, Global Change Biol., 14, 2178–2193, doi:10.1111/j.1365-2486.2008.01635.x, 2008.

Wingate, L., Ogée, J., Cuntz, M., Genty, B., Reiter, I., Seibt, U., Yakir,D., Maesyk, K., Pendall, E. G., Barbour, M. M., Mortazavi, B., Burlett, R., Peylin, P., Miller, J., Mencuccini, M., Shim, J. H., Hunt, J. Grace, J.: The impact of soil microorganisms on the global budget of δ^{18}O in atmospheric CO_2 Proc. Natl. Acad. Sci., 106, 22411–22415, doi:10.1073/pnas.0905210106, 2009.

WMO: Report of the 16th WMO/IAEA Meeting of Experts on Carbon Dioxide, Other Greenhouse Gases and Related Tracers Measurement Techniques (GGMT-2011): Wellington, New Zealand, 25–28 October 2011, GAW Report No. 206, available at: http://www.wmo.int/pages/prog/arep/gaw/gaw-reports.html (last access: 23 October 2014), Welligton, New Zealand, 2012.

Wunch, D., Toon, G. C., Blavier, J.-F., Washenfelder, R., Notholt, J., Connor, B., Griffith, D. W. T.. and Wennberg, P. O.: The Total Carbon Column Observing Network (TCCON). Phil. Trans. Roy. Soc. A, 369, 2087–2112, 2011.

Yakir, D. and Wang, X.-F.: Fluxes of CO_2 and water between terrestrial vegetation and the atmosphere estimated from isotope measurements, Nature, 380, 515–517, doi:10.1038/380515a0, 1996.